



# Effect of poly(3,4-ethylenedioxythiophene) (PEDOT) in carbon-based composite electrodes for electrochemical supercapacitors

Chunhong Lei, Peter Wilson, Constantina Lekakou\*

Division of Mechanical, Medical, and Aerospace Engineering, Faculty of Engineering and Physical Sciences, University of Surrey, Guildford GU2 7XH, UK

## ARTICLE INFO

### Article history:

Received 25 January 2011

Received in revised form 17 March 2011

Accepted 27 March 2011

Available online 6 April 2011

### Keywords:

Supercapacitor

EDLC

PEDOT:PSS

Activated carbon

## ABSTRACT

Electrochemical double layer supercapacitor cells were fabricated and tested using composite electrodes of activated carbon with carbon black and poly(3,4-ethylenedioxythiophene) (PEDOT), and an organic electrolyte 1 MTEABF<sub>4</sub>/PC solution. The effect of PEDOT on the performance of the EDLC cells was explored and the cells were characterised by electrochemical impedance spectroscopy (EIS), cyclic voltammetry and galvanostatic charge–discharge. A generalised equivalent circuit model was developed for which numerical simulations were performed to determine the properties and parameters of its components from the EIS data. It was found that the proposed model fitted successfully the data of all tested cells. PEDOT enhanced the electrode and cell capacitance via its pseudo-capacitance effect up to a maximum value for an optimum PEDOT loading and greatly increased the energy density of the cell while the maximum power density has been still maintained at supercapacitor levels. Furthermore, PEDOT replaced PVDF as a binder and harmful solvent release was reduced during electrode processing. Activated carbon–carbon black composite electrodes with PEDOT as binder were found to have specific capacitance superior to that of activated carbon–carbon black electrodes with PVDF binder.

© 2011 Elsevier B.V. All rights reserved.

## 1. Introduction

Supercapacitors, including electrochemical double layer capacitors (EDLCs) and redox or pseudo-capacitors, are generally fast charging energy-storage devices with power and energy densities performance between traditional capacitors and batteries. They can be used as alternative or complementary power sources in various applications including telecommunication devices, standby power systems, portable electronic devices and electric hybrid vehicles [1]. An EDLC stores the energy by accumulating the opposite charges on the thin double layer (5–10 Å) [2] at the interface between the porous electrode and the electrolyte through electrostatic force. Carbonaceous materials such as aerogel [3,4] and powder [5,6] are the most commonly used electrode materials in EDLC devices due to carbon's high surface area, chemical and thermal stability, relatively low cost and low environmental impact. Carbonaceous materials are usually activated [4,7] to produce a large porous surface area before being used for EDLC electrodes. On the other hand, the activation of carbon results in a lower electrical conductivity, usually 0.1–1.0 S cm<sup>-1</sup>, due to its high porosity and high surface area [8,9]. This large resistance inevitably results in an increase in power loss and energy dissipation. To improve the conductivity of carbon electrodes, conductive fillers, like carbon

nanotubes (CNTs) [10,11] and carbon black [12] can be added. 5% carbon black (CB) was mixed into AC to increase its conductivity [12] although high loading of CB in AC would induce a deterioration of the total capacitance due to the small surface area of the CB.

A pseudo-capacitor stores energy through relatively fast and reversible faradaic (redox) processes in a redox-active material at characteristic potentials. Conducting polymers, such as polyacetylene, polypyrrole, polyaniline, polythiophene, and their derivatives, are amongst the more promising materials for a polymer-based pseudo-capacitor [13]. Conducting polymers are able to store charge, not only in the electrical double layer, but also throughout the body of the polymer by rapid faradaic charge transfer i.e. a three-dimensional charge storage mechanism resulting in far higher capacity. However, the redox reaction in pseudo-capacitors is a slower process compared with the double layer process in EDLCs and, hence, the pseudo-capacitor has lower charge/discharge performance than an EDLC capacitor. One solution is to incorporate conducting polymers into the carbon electrode which has been shown to increase its capacitance while maintaining high level of power density [14,15].

Amongst conducting polymers, poly(ethylenedioxythiophene) (PEDOT) exhibits not only a high conductivity but also an unusual stability in the oxidized state, being considered as perhaps the most stable conducting polymer currently available [16] and, therefore, many researchers have studied PEDOT as the electrode material for supercapacitors [17–19].

\* Corresponding author. Tel.: +44 0 14 83 68 96 22; fax: +44 0 14 83 68 62 91.  
E-mail address: [C.Lekakou@surrey.ac.uk](mailto:C.Lekakou@surrey.ac.uk) (C. Lekakou).

**Table 1**  
Activated carbon composite electrodes for symmetric EDLCs.

Electrode	Carbon black (w/w%) <sup>a</sup>	PVDF (w/w%) <sup>a</sup>	PEDOT (w/w%) <sup>a</sup>
ACB	5	5	0
ACBP5	5	0	5
ACBP10	5	0	10

<sup>a</sup> Weight percentage to the total carbon composite.

PEDOT/carbon composite as electrodes for supercapacitors with high energy and power density have been reported [19,20]. But all the PEDOT reported in the PEDOT/carbon composite electrodes was synthesized in situ on carbon materials by electrochemical or chemical-polymerization from EDOT. It should be noted that although in situ synthesised PEDOT composite electrodes can have higher conductivity than the ones from mechanically blending the ingredients, the increased process complexity and longer manufacturing times render this an unfeasible route for mass-production.

In this study, a PEDOT/carbon composite electrode was fabricated by mechanical blending with a low concentration of PEDOT, which also acted as a binder. The effect of PEDOT on the performance of carbon composite electrodes for supercapacitor devices was explored, where the carbon composite base was activated carbon (AC) and 5% carbon black (CB). A commercial aqueous PSS doped PEDOT colloidal solution was used. The advantage of this aqueous PEDOT is that, after drying, the PEDOT/PSS film is highly conducting, mechanically durable, and insoluble in common solvents. When PEDOT was distributed in the AC matrix, AC should act as a scaffold, giving PEDOT a high surface-to-volume ratio, which improves both the energy and power density of the PEDOT itself through the increased surface area and by limiting the distance over which ion diffusion inside the PEDOT polymer body occurs. This aqueous PEDOT solution can work as a binder to replace conventional insulating binders such as PTFE and PVDF, reducing the resistance of the electrode and avoiding harmful solvents being released during electrode processing. The supercapacitor cells were assembled in a symmetric electrode configuration and 1 M tetraethylammonium tetrafluoroborate ( $\text{Et}_4\text{NBF}_4$  or  $\text{TEABF}_4$ ) in propylene carbonate (PC) was used as electrolyte.  $\text{TEABF}_4/\text{PC}$  electrolyte is widely used in batteries and capacitors as it allows a high electrochemical window of more than 3 V [1,21,22]. The capacitor cells were subjected to electrochemical impedance spectroscopy (EIS), cyclic voltammetry (CV) and galvanostatic charge–discharge (GCD) tests. The data obtained were used to fit a generalised equivalent circuit model for each type of cell.

## 2. Experimental details

The composite electrodes were prepared from a blend of activated carbon (AC) (Sigma–Aldrich), poly(3,4-ethylenedioxythiophene)–poly(styrenesulfonate) (PEDOT–PSS) (Sigma–Aldrich, 1.3 wt% dispersion in  $\text{H}_2\text{O}$ ), carbon black (acetylene) (Alfa Aesar) and poly(vinylidene fluoride) (PVDF) (Sigma–Aldrich). All the chemicals were used without further treatment. Electrodes were constructed according to the ratios in Table 1 and were mixed thoroughly in PEDOT solution, or 1-methyl-2-pyrrolidinone (NMP) if PVDF was used, to form a slurry. The slurry was then coated onto aluminium foil using an Elcometer Film Applicator. The film was then dried in an oven at 200 °C for

**Table 2**  
Parameters of the generalised equivalent circuit model for each type of cell (2 cm<sup>2</sup>) derived from the best numerical fitting of the experimental data of Nyquist plots.

Cell with electrodes	L1 ( $\mu\text{H}$ )	R1 ( $\Omega$ )	CPE1:Q1 ( $\text{Ss}^{n1}$ )	CPE1:n1	R2 ( $\Omega$ )	CPE3:Q3 ( $\text{Ss}^{n3}$ )	CPE3:n3	CPE2:Q2 ( $\text{Ss}^{n2}$ )	CPE2:n2
ACB	1.50	2.05	$1.1 \times 10^{-3}$	0.87	3.1	1.10	0.1	1.59	0.947
ACBP5	1.35	2.05	$3.1 \times 10^{-3}$	0.94	6.1	1.15	0.4	3.4	0.995
ACBP10	1.35	2.24	$1.0 \times 10^{-3}$	0.93	5.35	1.10	0.3	2.35	0.956

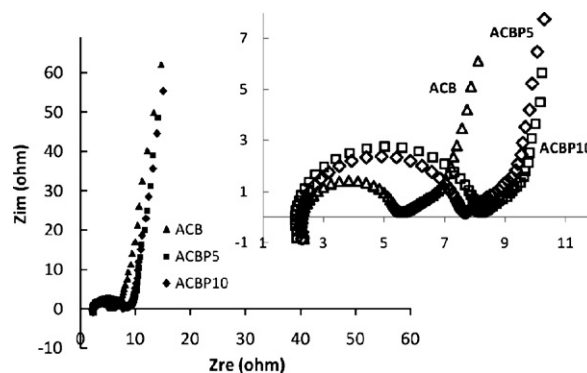


**Fig. 1.** (a) Nyquist plots for the EDLC cells with ACB, ACBP5 and ACBP10 electrodes at a dc bias of 0.2 V and sinusoidal signal of 20 mV over the frequency range 1000 kHz–0.01 Hz.  $Z_{re}$ : real impedance.  $Z_{im}$ : imaginary impedance. Inset shows an enlarged scale of the plot.

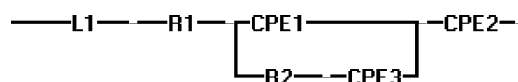


**Fig. 2.** Generalised equivalent circuit model used for all supercapacitor cells in this study, consisting of an inductor L1, two resistors R1 and R2, and three constant phase elements CPE1, CPE2 and CPE3.

2 h. The dried carbon film had a thickness of about 150  $\mu\text{m}$  and a loading of  $\sim 5.5 \text{ mg cm}^{-2}$ . All the composite electrodes tested are listed in Table 1.

The capacitor cells were assembled by placing two rectangular strips of carbon composite coated Al film with the carbon sides face to face. A piece of filter paper soaked with electrolyte solution was placed in between the strips as a separator. The electrodes overlap area defined the working area which was fixed to 2 cm<sup>2</sup> in all the devices. Finally the device assembly was sealed in a plastic “bag” by vacuum.

The electrolyte was 1 M  $\text{Et}_4\text{NBF}_4$  (Sigma–Aldrich, purity 99%) in PC (Sigma–Aldrich, anhydrous, purity 99.7%).

The performances of different EDLC cells were characterized by EIS, CV, and GCD tests, using a VersaSTAT MC analyser. The devices were characterized in a 2-terminal configuration, no reference electrode was used in the tests.

## 3. Results and discussion

### 3.1. Electrochemical impedance spectroscopy analysis and equivalent circuit models

The EIS measurements on the cells were carried out at a DC bias of 0.2 V with a sinusoidal signal of 20 mV over the frequency range from 1 MHz to 10 mHz. Fig. 1 shows the corresponding Nyquist plots for the three devices with ACB, ACBP5 and ACBP10 electrodes. The Nyquist plots were used for the fitting of a generalised equivalent circuit model presented in Fig. 2, consisting of an inductor L1 affecting the cell behaviour only at the highest frequencies, an equivalent series resistance R1, a parallel resistance R2, and three constant phase elements CPE1, CPE2, CPE3. A constant phase ele-

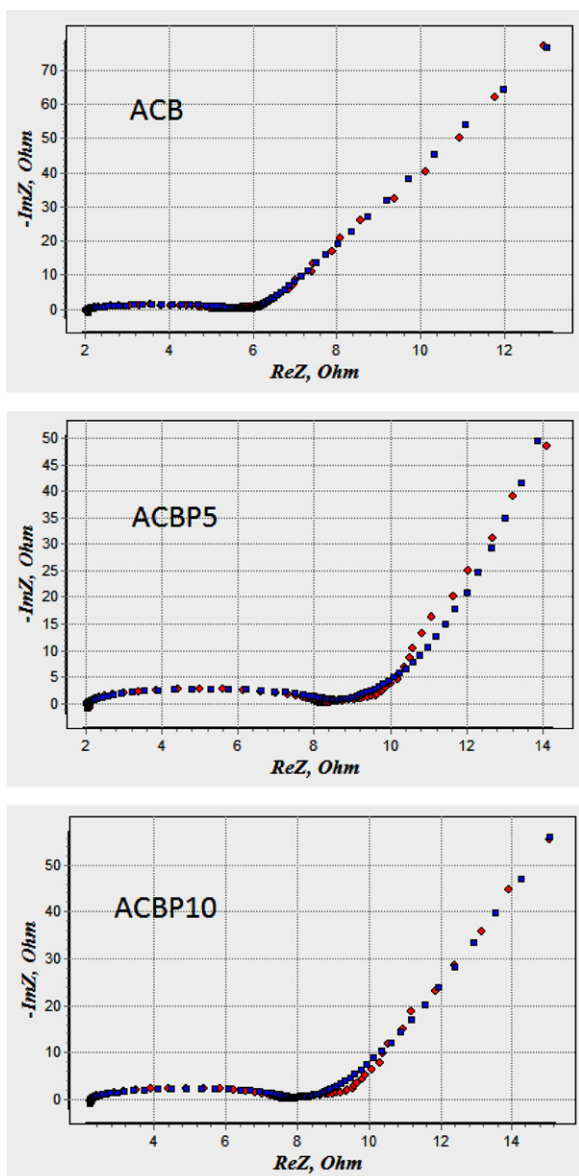


Fig. 3. Experimental EIS data (♦) and predictions (■) of the generalised equivalent circuit model with parameter values displayed in Table 2.

ment (CPE) is described by the equation

$$z = \frac{1}{Q(j\omega)^n} \quad (1)$$

For  $n=1$  the CPE is a capacitor with capacitance  $Q$ . For  $n=0$  the CPE is a resistor with resistance  $1/Q$ . Table 2 presents the values of the parameters of the generalised equivalent circuit model for each type of tested supercapacitor cell, where these parameters were derived from a best fit of the data of the corresponding Nyquist plots in Fig. 1 using the EIS Spectrum Analyser® software. Fig. 3 displays the Nyquist plots of the experimental data and the predictions of the corresponding equivalent circuit models using the parameters from Table 2.

The first capacitor behaviour in EIS occurs in the region of high-to-medium frequencies illustrated by the semi-circle in the Nyquist plots in Figs. 1 and 3 and represented by the constant phase element CPE1 in the generalised equivalent circuit model in Fig. 2. At these high-to-medium frequencies only small amounts of charge complexes in electrolyte can overcome the activation energy to migrate with the alternating potential, hence the capacitance is low devel-

oped by the moving electrolyte ions close to the Helmholtz plane represented by an interfacial contact capacitance ( $C_c$ ) and charge transfer resistance ( $R_{ct}$ ) within the micropores of porous carbon [23–25]. Lower  $R_{ct}$  indicates better electrolyte pore accessibility. The closer the value of  $n$  is to one in a CPE in the equivalent circuit model the closer to capacitor rather than resistor the element is. CPE1 has high  $n1$  values for all cells (Table 2) indicating capacitor behaviour, especially for the cells with PEDOT in the carbon composite electrode at 5 and 10% loadings. More specifically ACBP5 at 5% PEDOT loading has the highest CPE1 capacitance (semi-circle region).

The semicircle has two intersection points on the real axis: the first  $Z_{re}$  intersection point at the left end of the semicircle represents the ohmic resistance of the bulk electrolyte solution modeled by the equivalent-in-series resistance  $R1$  in the equivalent circuit model in Fig. 2, which is approximately the same for all three types of capacitor cells. The diameter of the semi-circle represents the charge transfer resistance,  $R_{ct}$ , modeled mainly by the in-parallel resistance  $R2$  in the equivalent circuit model: the results in Table 2 demonstrate that it is lowest in the case of ACB electrodes and it increases when PEDOT is added, indicating worse pore accessibility by the electrolyte in the latter case. This indicates that the addition of PEDOT has reduced the rate of charge transfer presumably by constricting part of the micro-pores of the AC and forming a higher resistance interface between the AC particles and the PEDOT. In the case of ACB which has PVDF binder, although PVDF is an insulator, when the electrode is dried at 200 °C PVDF melts and shrinks through surface tension to expose AC micropores and to improve carbon particle–particle contact; as a result  $R_{ct}$  is smaller in ACB than in the electrodes with PEDOT. This is illustrated in Fig. 4 which presents SEM micrographs of the (a) ACB and (b) ACBP5 electrodes. The larger, irregular particles are the AC particles which are covered by clusters of the small carbon black particles that are embedded in the binder. In the case of (a) ACB, the shrinkage of the PVDF binder has compressed the carbon black particles to form denser clusters of carbon black that would improve carbon particle-to-particle contact and expose AC micropores. In the case of (b) ACBP5, PEDOT acting as a binder shrinks less and allows for large clusters of carbon black particles embedded in the PEDOT matrix and covering more surface area of AC. Furthermore, it was found that the ACB coating was somehow easy to be peeled off the Al foil whereas the PEDOT formed a robust and flexible coating with ACB in ACBP5 and ACBP10 and these coatings were hard to peel off the Al foil that has been used as the outer electrode in this study.

On the right side of the semicircle in the Nyquist plots in Fig. 1, the equivalent circuit model in Fig. 2 includes a constant phase element CPE3, for which the low value  $n3=0.1$  determined from the fit of the equivalent circuit model to the EIS data for the ACB-based cell, indicates that CPE3 can be approximated by a resistor in the ACB-based cell of approximately  $(1 \times 10)^{-1} \Omega = 0.9 \Omega$  that really adds to the value of the in-parallel resistance  $R2$ . In the case of the ACBP5-based cell, with the electrode containing 5% PEDOT, it was determined that the phase element CPE3 could be fitted to the EIS data with  $n3=0.4$  which means that CPE3 in ACBP5 can be approximated by a  $\sim 45^\circ$  Warburg element which represents the ion diffusion into the bulk of the electrode through pores of varying size [24].

Finally, at lower frequencies, the EIS curve is almost vertical (Fig. 1), indicating the capacitive nature of the device. This is represented by the constant phase element CPE2 in the equivalent circuit model, in which  $n2 \approx 1$  for all types of cells in Table 2 indicating a good capacitor with capacitance  $Q2$ . Furthermore, the 5% w/w PEDOT composition more than doubles the capacitance of CPE2 in comparison with that of the ACB based cell and in fact it seems to be the best PEDOT content for CPE2 to be the ideal capacitor ( $n2 = 1$ ) and have the highest capacitance  $Q2$ .

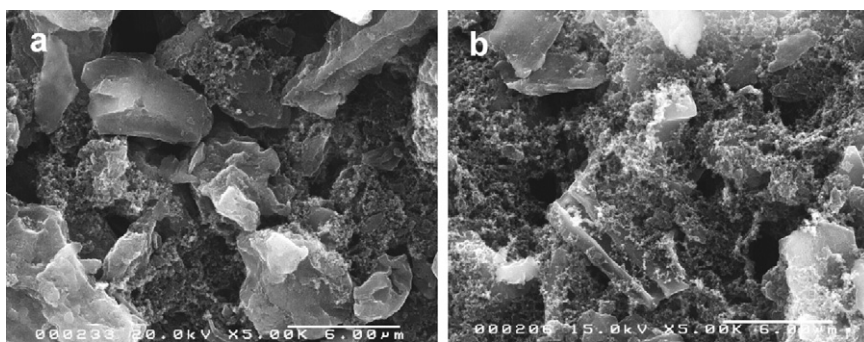


Fig. 4. SEM micrographs of (a) ACB and (b) ACBP5 electrodes.

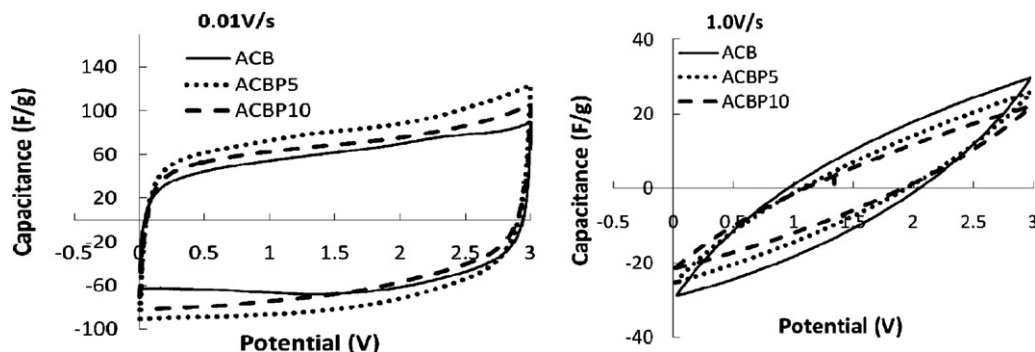


Fig. 5. Cyclic voltammograms of EDLC cells with ACB, ACBP5 and ACBP10 electrodes using 1 M TEABF<sub>4</sub>-PC electrolyte at two extreme sweep rates: (a) 0.01 V s<sup>-1</sup>, (b) 1.0 V s<sup>-1</sup>.

### 3.2. Cyclic voltammetry

In order to estimate the capacitance of the cells and stability of the electrolyte, cyclic voltammetry (CV) was carried out for the three types of cells in a series of sweeps at a rate from 0.01 V s<sup>-1</sup> to 1.0 V s<sup>-1</sup> between 0 and 3 V. Fig. 5 displays two typical CV curves at two extreme scan rates, where the specific capacitance of one electrode is given by the following equation:

$$C = \frac{2i}{mv} \quad (2)$$

where  $i$  is the current,  $v$  is the scan rate and  $m$  is the mass of one electrode. The curves are regular and reproducible, indicating good stability of the electrolyte in this operating voltage range. At low scan rate, all electrodes gave a CV shape closely resembling a rectangle. The capacitance value is in the order of ACBP5 > ACBP10 > ACB, indicating that addition of PEDOT in AC can increase the cell capacitance to a maximum and then decrease as the concentration of PEDOT increases, which is due to the pseudo-capacitance contribution of PEDOT, limited by slower ion diffusion at high PEDOT concentration. The capacitance values at slow scan

rate are consistent with the values of  $Q_2$  of the constant phase element CPE2 (almost capacitor as discussed in Section 3.1) in Table 2, where  $Q_2$  represents the cell capacitance at low frequencies in the EIS data. As PEDOT is increased from 5% in ACBP5 to 10% in ACBP10, CPE3, which characterises ion diffusion through different size pores, has  $n_3$  displayed in Table 2 decreasing from  $n_3 = 0.4$  in ACBP5 to  $n_3 = 0.3$  in ACBP10, demonstrating that CPE3 is more resistor than capacitor in ACBP10, i.e. the higher PEDOT concentration leads to slower ion diffusion which decreases the overall retained charge and, hence, capacitance in ACBP10. Although the addition of PEDOT has increased the capacitance, no obvious redox peak of faradic contribution can be seen in the range of 0–3 V; this does not mean that there is no redox reaction as conducting polymers contain a broad range of energy states, which can result in a wide redox peak [26,27]. In addition, as the CV was performed on the full EDLC cell, oxidation and reduction can happen at the positive and negative electrodes at different times which may have the effect of smoothing the redox peak of the full cell.

At high sweep rates the CV curves of all electrodes were severely distorted to slim, leaf like shapes due to ions being able

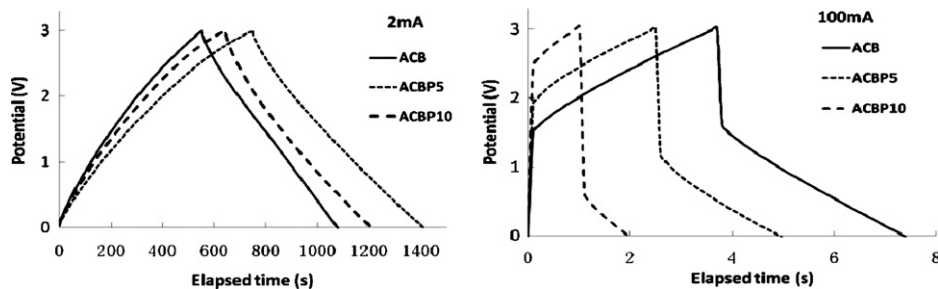


Fig. 6. Galvanostatic charge–discharge curves of EDLC cells with ACB, ACBP5 and ACBP10 electrodes using 1 M TEABF<sub>4</sub>-PC electrolyte at two extreme constant currents: (a) 2 mA, (b) 100 mA.



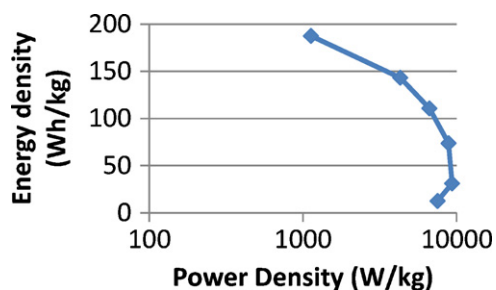


Fig. 7. Ragone plot for the ACBP5 supercapacitor cell.

to only arrive at shallow positions within pores and the increasing diffusion resistance from the migration friction between the charge-complexes and the PC molecules, with the increasing sweep rate. The capacitance value is in the order of  $ACB > ACBP5 > ACBP10$ , due to the higher charge transfer resistance as the PEDOT concentration increases and due to the redox process being comparatively slow. The high scan rate cyclic voltammetry tests at  $1 \text{ V s}^{-1}$  up to 3 V and back to 0 V could be considered equivalent to a frequency of 0.16 Hz for triangular AC function which means that for all cells this is the regime controlled by the rate of ion diffusion through pores of different sizes, i.e. the branch of charge transfer resistance represented by  $R_2$  and CPE3 in the equivalent circuit model of Fig. 2. Adding PEDOT seems to incur a higher transfer resistance  $R_2$  than in ACB (see Table 2) when the ACBP5-based cell is compared to the ACB-based cell, while 10% PEDOT slows down ion diffusion ( $n_3 = 0.3$ ) compared to the case of the ACBP5-based cell ( $n_3 = 0.4$ ). Increasing the electrical conductivity of PEDOT might improve the situation.

### 3.3. Galvanostatic charge–discharge tests

In order to examine the device performance including the dependence of the capacitance on the current density and evaluate the cell capacitance with respect to its power, charge–discharge cycling between 0 and 3 V at various currents from 2 mA to 100 mA was carried out. Fig. 6 displays two typical charge–discharge plots at  $1 \text{ mA cm}^{-2}$  and  $50 \text{ mA cm}^{-2}$ . At the low current density,  $1 \text{ mA cm}^{-2}$  (or 2 mA current), all electrodes showed triangular charge–discharge curves, suggesting that the electrodes tested have no obvious redox reaction, which is consistent with the CV measurements. The performance (time elapsed during charge–discharge) of the three electrodes is in the order  $ACBP5 > ACBP10 > ACB$ , which is consistent with their CV behaviour at low scan rates. At the high current density of  $50 \text{ mA cm}^{-2}$  (or 100 mA current), the performance of the electrodes is in the order  $ACB > ACBP5 > ACBP10$ , due to the increased internal resistance as the content of PEDOT increased. The IR drop at the turning point of the charge–discharge line, which indicates the energy loss due to the internal or equivalent series resistance (ESR) [28], was enlarged at the higher current density. The IR drop of the three electrodes is in the order  $ACB < ACBP5 < ACBP10$ , indicating that PEDOT increased the internal resistance, by coating the carbon particles. Although PEDOT is more conductive than PVDF, it does not shrink like PVDF at high temperature. However, PEDOT can be modified to increase its conductivity by adding a cosolvent such as DMSO [29].

The results of various CV and charge–discharge tests for the ACBP5 cell were assembled and converted to an energy density–power density Ragone plot for this single cell, which is presented in Fig. 7. The plot illustrates that the addition of 5% w/w PEDOT to the activated carbon–5% w/w carbon black composite electrode increases the capacitance leading to increased energy density of the supercapacitor cell approaching  $200 \text{ Wh kg}^{-1}$  in our

tests whereas the power density of the single small cell reaches a maximum value at  $10 \text{ kW kg}^{-1}$ .

## 4. Conclusions

This study has investigated the effect of PEDOT:PSS on an activated carbon–5% w/w carbon black composite electrode used in supercapacitor cells with 1 M TEABF<sub>4</sub>–PC electrolyte. The fabricated cells were subjected to electrochemical impedance spectroscopy (EIS), cyclic voltammetry and charge–discharge tests. A generalized equivalent circuit model with equivalent-in series-resistance, in-parallel resistance and three constant phase elements (CPEs) was fitted successfully to the EIS results for all types of cells.

In general, the addition of PEDOT:PSS enhanced the capacitance of the cell to a maximum at 5% w/w PEDOT, due to the additional pseudo-capacitance of PEDOT. This is beneficial for capacitors used in low frequency applications, which still includes a large range of applications such as automotive energy storage. In fact, the capacitance of the CPE2 component of the equivalent circuit model was doubled by adding 5% w/w PEDOT, where CPE2 is the supercapacitor component functioning in the low frequency range. The work also demonstrated the feasibility of using PEDOT as a binder for AC which also reduces the release of harmful organic solvents during the electrode fabrication process. On the other hand, PEDOT contributed to a reduction in charge mobility and increase of the charge transfer resistance i.e. the parallel resistance in the equivalent circuit model.

## Acknowledgments

This research was supported by the Engineering and Physical Sciences Research Council (EPSRC). We would like to thank Prof. Joe Keddie in the Physics Department at the University of Surrey for the courtesy of facility usage in his laboratory.

## References

- [1] A. Burke, J. Power Sources 91 (2000) 37.
- [2] Y. Zhang, H. Feng, X. Wu, L. Wang, A. Zhang, T. Xia, H. Dong, X. Li, L. Zhang, Int. J. Hydrogen Energy 34 (2009) 4889.
- [3] J. Li, X. Wang, Q. Huang, S. Gamboa, P.J. Sebastian, J. Power Sources 158 (2006) 784.
- [4] B. Fang, L. Binder, J. Power Sources 163 (2006) 616.
- [5] V. Khomenko, E. Raymundo-Piñero, F. Beguin, J. Power Sources 177 (2008) 643.
- [6] C.-C. Hu, C.-C. Wang, F.-C. Wu, R.-L. Tseng, Electrochim. Acta 52 (2007) 2498.
- [7] H. Pröbstle, M. Wiener, J. Fricke, J. Porous Mater. 10 (2003) 213.
- [8] R. Chandrasekaran, Y. Soneida, J. Yamashita, M. Kodama, H. Hatori, J. Solid State Electrochem. 12 (2008) 1349.
- [9] A.G. Pandolfo, A.F. Hollenkamp, J. Power Sources 157 (2006) 11.
- [10] T. Bordjiba, M. Mohamedi, L.H. Dao, J. Power Sources 172 (2007) 991.
- [11] G. Lv, D. Wu, R. Fu, Z. Zhang, Z. Su, J. Non-Cryst. Solids 354 (2008) 4567.
- [12] Y.J. Kim, Y.A. Kim, T. Chino, H. Suezaki, M. Endo, M.S. Dresselhaus, Small 2 (2006) 339.
- [13] G.A. Snook, P. Kao, A.S. Best, J. Power Sources 196 (2011) 1.
- [14] M. Mastragostino, R. Paraventi, A. Zanelli, Supercapacitors based on composite polymer electrodes, J. Electrochem. Soc. 147 (2000) 3167.
- [15] M. Selvakumar, D. Krishna Bhat, J. Appl. Polym. Sci. 107 (2008) 2165.
- [16] B.L. Groenendaal, F. Jonas, D. Freitag, H. Pielartzik, J.R. Reynolds, Adv. Mater. 12 (2000) 481.
- [17] K.S. Ryu, Y.-G. Lee, Y.-S. Hong, Y.J. Park, X. Wu, K.M. Kim, M.G. Kang, N.-G. Park, S.H. Chang, Electrochim. Acta 50 (2004) 843.
- [18] A. Laforge, J. Power Sources 196 (2011) 559.
- [19] R. Liu, I.S. Cho, S.B. Lee, Nanotechnology 19 (2008) 215710.
- [20] T.L. Kelly, K. Yano, M.O. Wolf, ACS Appl. Mater. Interfaces 1 (2009) 2536.
- [21] A. Laheäär, H. Kurig, A. Jänes, E. Lust, Electrochim. Acta 54 (2009) 4587.
- [22] F.-Q. Li, Y.-Q. Lai, Z.-A. Zhang, H.-Q. Gao, J. Yang, Acta Phys. Chim. Sin. 24 (2008) 1302.
- [23] K. Hung, C. Masarapu, T. Ko, B. Wei, J. Power Sources 193 (2009) 944.
- [24] C. Masarapu, H.F. Zeng, K.H. Hung, B. Wei, ACS Nano 3 (2009) 2199.
- [25] B. Fang, L. Binder, Electrochim. Acta 52 (2007) 6916.
- [26] S.W. Zhang, G.Z. Chen, Energy Mater. 3 (2008) 186.
- [27] J.H. Chae, K.C. Ng, G.Z. Chen, Proc. IMechE A: J. Power Energy 224 (2010) 479.
- [28] A. Izadi-Najafabadi, S. Yasuda, K. Kobashi, T. Yamada, D.N. Futaba, H. Hatori, M. Yumura, S. Iijima, K. Hata, Adv. Mater. 22 (2010) E235.
- [29] H.J. Lee, J. Lee, S.-M. Park, J. Phys. Chem. B 114 (2010) 2660.